Progress In Electromagnetics Research C, Vol. 86, 257–267, 2018

A Broadband Negative Epsilon Fractal Metamaterial Unit Cell for Coaxial Notch Filter Applications

Kathryn Smith* **and Ryan Adams**

Abstract—Herein is presented a two-dimensional negative permittivity unit cell for coaxial notch filter applications. This novel unit cell is developed through simulation in the context of an ideal infinite parallel plate waveguide, and preliminary implementation is demonstrated through simulation and measurement in a finite parallel plate waveguide. Finally, the unit cells are incorporated as an in-line notch filter in a coaxial transmission line, and their efficacy is demonstrated through simulation and measurement. The unit cell developed for this application was formed as a broadband fractal expansion of the traditional capacitively loaded strip. A partial repetition of the basic CLS I-shape was inserted in the capacitive gap on either side of the structure. This new unit cell was developed and simulated in HFSS using an incident TEM wave excitation in a parallel plate waveguide, and was shown to have two resonant frequencies of interest. The first resonance produces a wide bandwidth of negative permittivity (29.5%) from 1.3 GHz to 1.75 GHz; the second produces a region of negative permeability from 2.05 GHz to 2.45 GHz, a bandwidth of 17.8%. The current on the structure at each of these frequencies is presented, along with the pertinent fields in the waveguide. The effects of various alterations to the basic shape of the unit cell are also presented.

1. INTRODUCTION

Electromagnetic metamaterials are periodic arrays of unit cells that are engineered to provide unique effective material properties such as negative permeability and negative permittivity [1, 2]. The mechanism by which these properties are achieved is generally tied to the self-resonance of the structures being used, which results in a limited bandwidth of performance. One of the most effective unit cell geometries to achieve negative permittivity is the electric disk resonator (EDR) [3] (see Fig. 1(a)). This structure consists of two parallel disks connected by a thin wire. The desired negative permittivity response of such unit cells occurs over a narrow band of frequencies where the capacitance between the two disks resonates with the inductance of the wire. The area of the disks and the radius of the wire are used to design the operative frequency so that the EDR is electrically small. Unfortunately, this structure is not easily manufactured because of its three dimensional shape. To simplify manufacturing and implementation, this structure may be approximated with a capacitively loaded strip [4] (see Fig. 1(b)), which is simply a two-dimensional rendering of the three-dimensional geometry. This 2D structure has been explored and found to effectively induce negative permittivity, although its bandwidth is narrower, and the field interaction is weaker than the three-dimensional version.

The efficacy of fractal geometries in producing enhanced bandwidth in resonant structures such as antennas and metamaterials has been demonstrated in [5–11], among others. Fractals exhibit self-similarity, which leads to multiband behavior as similar current patterns form in various portions of the structure at different frequencies. If these multiple bandwidths are designed to occur at closely

Received 2 March 2018, Accepted 28 August 2018, Scheduled 8 September 2018
* Corresponding author: Kathryn Smith (ksmit351@uncc.edu).
The authors are with the Department of Electrical and Computer Engineering at the University of North Carolina at Charlotte, 9201 University City Blvd. Charlotte, NC, USA.

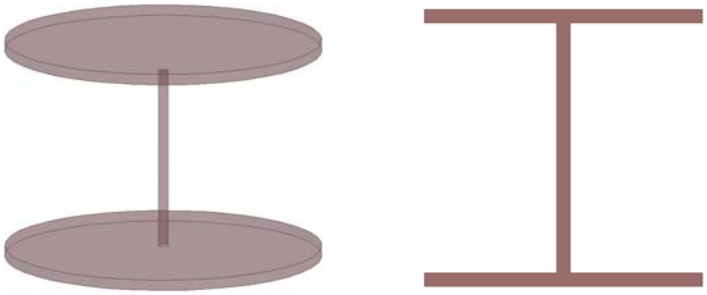

(a) (b)

Figure 1. (a) A three-dimensional EDR unit cell. (b) A two-dimensional CLS unit cell.

neighboring frequencies, they can overlap and induce broadband behavior. In [7], a fractal expansion of the basic I-shape of the capacitively loaded strip was proposed with additional replicas of the "I" that would resonate at different frequencies. This fractal structure was shown to provide multiple stopbands, but it lacked continuous bandwidth. The current work presents a novel unit cell geometry combining the work of [7] and [12], with modification of the individual lengths of each part of the geometry, as well as addition of discrete capacitively coupled resonators, to significantly broaden the operative bandwidth of this structure. The utility of the sharp, strong reflection obtained from this single-negative structure over its operative bandwidth is demonstrated through implementation in a notch filter. Preliminary simulation and measurement are performed in a parallel plate waveguide transmission line, and a final application is developed and measured in a coaxial transmission line section.

2. THE SINGLE UNIT CELL

Figure 2(a) shows a single unit cell of the fractal metamaterial structure under consideration. The conductive traces have a thickness of 0.035 mm, and are positioned on a substrate of FR-4 epoxy having a thickness of 0.790 mm. The I-shape is central to the structure, with four secondary I-shapes on the ends of the primary I-shape. Two additional I-shapes were added in the middle of each side and are capacitively coupled to the primary fractal structure. The lengths of each section were designed to maximize the bandwidth over which the effective permittivity was negative. To improve performance of this unit cell, and reduce overall size, the geometry of Fig. 2(a) was modified by truncation of the grayed-out sections to form the final structure shown in Fig. 2(b), where $L = 20\,\text{mm}$, $U = 22\,\text{mm}$, $g_1 = 5\,\text{mm}$, $g_2 = 0.5\,\text{mm}$, $g_3 = 3.67\,\text{mm}$, and all traces are 1 mm wide.

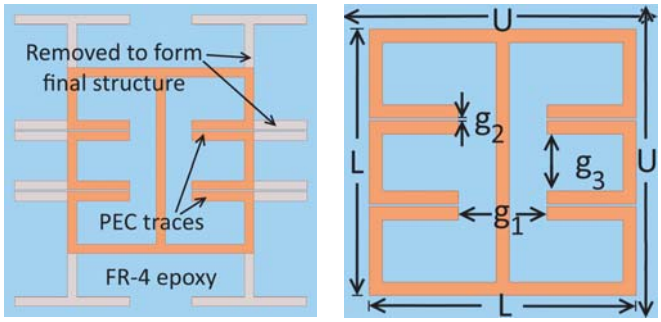

(a) (b)

Figure 2. (a) The complete fractal metamaterial unit cell. (b) The truncated fractal metamaterial unit cell, with dimensions $L = 20\,\text{mm}$, $U = 22\,\text{mm}$, $g_1 = 5\,\text{mm}$, $g_2 = 0.5\,\text{mm}$, $g_3 = 3.67\,\text{mm}$, where all traces are 1 mm wide.

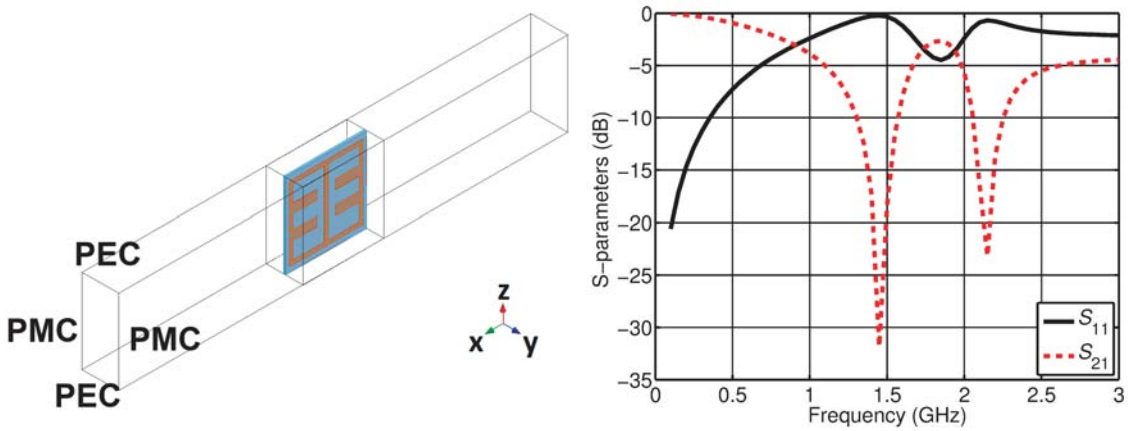

Figure 3. (a) HFSS model of the fractal metamaterial in a parallel plate waveguide. (b) The reflection and transmission resulting from simulation of the single fractal metamaterial unit cell.

A single unit cell having the geometry described above was simulated within a vacuum filled parallel plate waveguide using Ansys HFSS, as shown in Fig. 3(a). Parallel plate waveguide is commonly used for metamaterial characterization, because it supports TEM fields, and therefore the metamaterial in the parallel plate waveguide interacts with the field in a manner analogous to that of a metamaterial suspended in free space. The parallel plate waveguide model used in this simulation was 10 mm wide and 22 mm high. The horizontal sides at the top and bottom of the waveguide were defined as perfect electric conductor (PEC) and the vertical sides at the front and back were defined as perfect magnetic conductor (PMC).

The reflection and transmission resulting from simulation of this metamaterial are presented in Fig. 3(b). This figure reveals two resonant frequencies, characterized by high reflection. The first of these occurs at 1.45 GHz, where the unit cell size is slightly less than $\lambda_\circ/10$, and the second resonance occurs at 2.15 GHz, where the unit cell is approximately $\lambda_\circ/7$. The unit cell behavior at these resonant points is illustrated with the fields in the guide, as well as the surface currents on the unit cell, at each resonant frequency. Fig. 4(a) shows the currents on the unit cell at 1.45 GHz, viewed from the positive y axis, with excitation in the guide from the left. As shown, the highest concentration of current is on the center trace, with the return path on the left and right sides. This current pattern is analogous to that of a capacitively loaded strip (CLS) unit cell, which is known to exhibit negative permittivity [4]. Fig. 4(b) shows the electric field in the waveguide at 1.45 GHz, viewed from the positive y-axis. Excitation is again from the left. As shown, the incident field, which is pointing upward, reverses direction to point downward as it travels into the unit cell. The incident field also undergoes drastic attenuation, so that very little of the field penetrates to the right side of the unit cell; both images are consistent with the extracted negative permittivity and positive permeability.

Figures 4(c) and 4(d) show similar information for the second frequency of resonance. Fig. 4(c) shows the currents on the structure at 2.15 GHz, with excitation from the left. In this case, the current is concentrated in the left side of the structure, with the return path on the center and right side posts. This current pattern is analogous to that of an split ring resonator (SRR), which is a known negative-permeability structure. Fig. 4(d) shows the structure of the magnetic field in the guide at 2.15 GHz, viewed from the positive z-axis, with excitation from the left. As the electric field did at the previous resonance, the magnetic field exhibits a complete reversal as it passes into the unit cell. This figure also shows that the transmitted field is very small. Each of these results is consistent with negative permeability combined with positive permittivity.

The relative permeability and permittivity of this metamaterial structure were calculated directly from the simulated scattering parameters using the extraction algorithm described in [13]. Fig. 5(c) shows the real parts of the extracted relative permeability and relative permittivity. As expected from the field plots of Fig. 4, the first resonance is characterized by negative permittivity, and the second

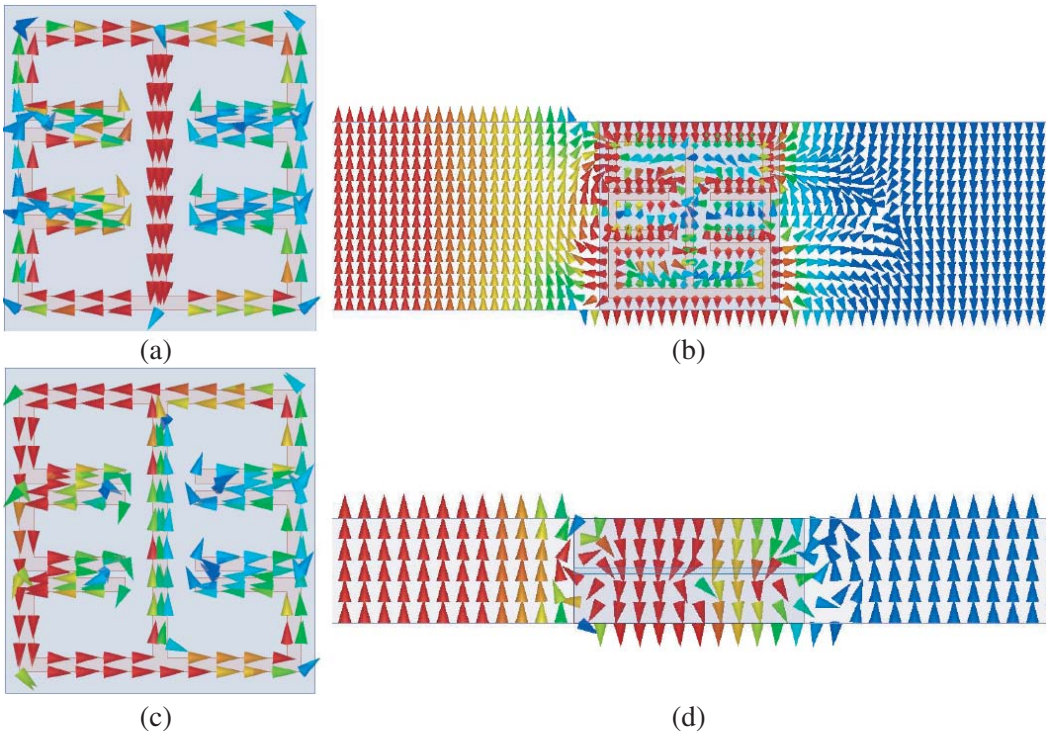

Figure 4. (a) The current on the structure at 1.45 GHz, viewed from the positive y direction. (b) The E-field inside the waveguide at 1.45 GHz, viewed from the positive y direction. (c) The current on the structure at 2.15 GHz, viewed from the positive y direction. (d) The H field inside the waveguide at 2.15 GHz, viewed from the positive z direction.

by negative permeability. Permittivity is negative in the range 1.3 GHz–1.75 GHz, corresponding to a bandwidth of 29.5%, and permeability is negative in the range 2.05 GHz–2.45 GHz, corresponding to a bandwidth of 17.8%. It is noteworthy that the value of the extracted effective permittivity is quite high far from resonance. For instance, at 100 MHz the extracted permittivity is 5.1. This is most likely due to the presence of metal in the parallel plate waveguide.

3. SIMULATION OF THREE UNIT CELLS

The single unit cell was then extended to three side-by-side structures, as shown in Fig. 5(a). The three unit cells were simulated in the same parallel plate waveguide model as discussed previously, where the height of the guide was 22 mm, the width was 10 mm, and the horizontal and vertical sides were defined as PEC and PMC, respectively.

Figure 5(b) shows the S-parameters resulting from this simulation. In this case, instead of exhibiting a single sharply defined resonance at 1.45 GHz, as in the case of the single unit cell, the first reflective region appears to consist of three closely spaced resonances at 1.25 GHz, 1.40 GHz, and 1.60 GHz. The second reflection remained a single point at 2.15 GHz. These changes are most likely a product of inter-elemental coupling between the three unit cells, as discussed in detail in [14]. Fig. 5(c) shows the extracted values of relative permeability and permittivity for the case of the three unit cells. As shown, this simulation has a region of negative permittivity from 1.25 GHz to 1.80 GHz, corresponding to a bandwidth of approximately 36%. This is a 6.5% increase over the single-cell simulation. The region of negative permeability extends from 2.05 GHz to 2.40 GHz, corresponding to a bandwidth of 15.7%. This is a decrease of 2.1% from the single-cell case.

To explore the significance of various features of the unit cell, two additional structures were simulated. In the first case, shown in Fig. 6(a), the two capacitively-loaded gaps in each of the left and right side posts have been replaced by a single vertically-centered capacitive gap, having the same

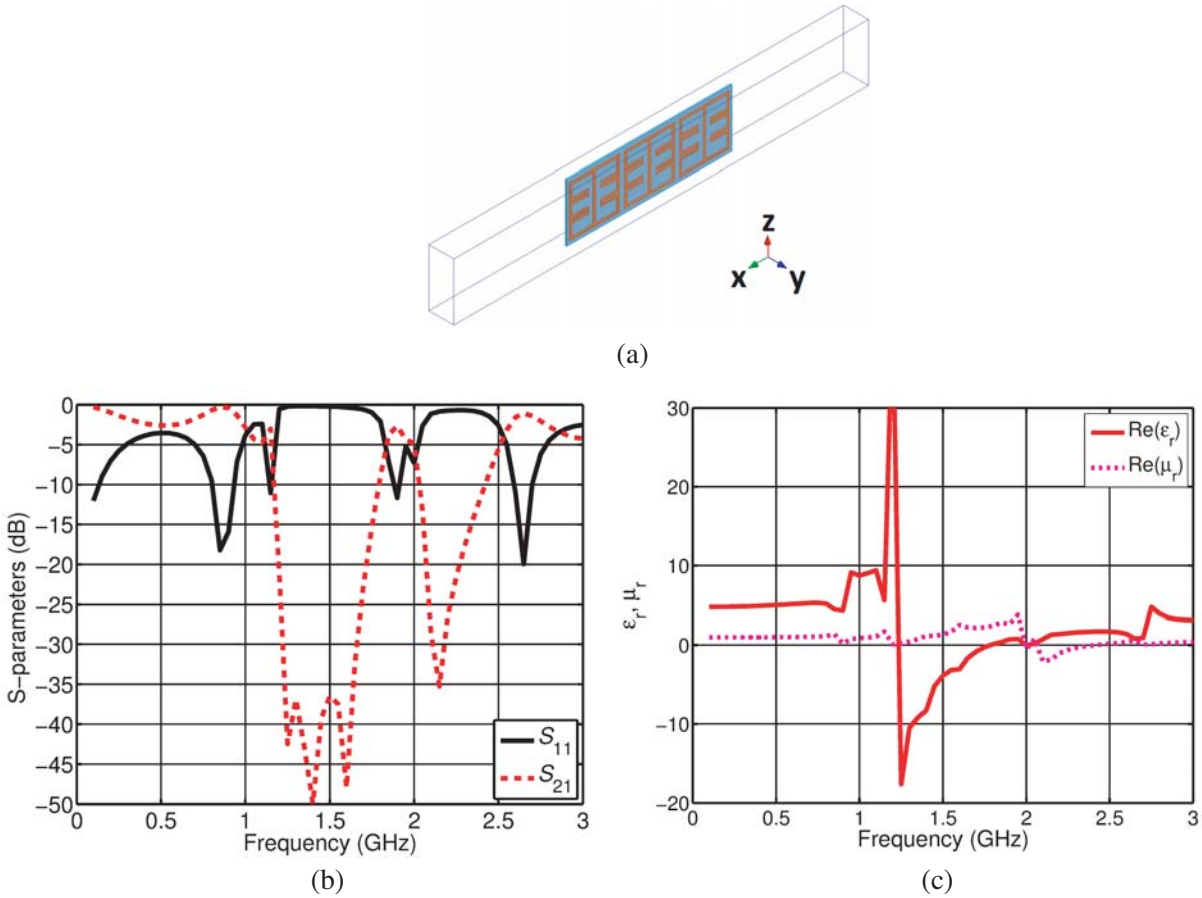

Figure 5. (a) Three fractal structures in the same waveguide as discussed previously. (b) S-parameters resulting from the simulation of three side-by-side fractal unit cells in a parallel plate waveguide. (c) Extracted real parts of effective permeability and permittivity, resulting from simulation of three side-by-side fractal unit cells in a parallel plate waveguide.

dimensions as original two. This structure resembles one presented in [15, 16]. The S-parameters and extracted permeability and permittivity resulting from this simulation are shown in Figs. 6(b) and 6(c). As shown in Fig. 6(b), this structure resonates at three frequencies: 1.05 GHz, 1.15 GHz, and 1.5 GHz. The extraction shown in Fig. 6(c) indicates that the first two resonances correspond to negative permittivity, which is continuous from 1.05 GHz to 1.25 GHz. The third resonance corresponds to negative permeability, which is demonstrated from 1.4 GHz to 1.8 GHz. By comparison of these results with those shown in Fig. 5(c), it can be seen that the effect of the second gap is to broaden the bandwidth of the electric response, and to strengthen the magnetic interaction.

In the second test case, shown in Fig. 7(a), the continuous part of the structure is identical to the original case, but the two detached gap resonators have been removed. As shown in Fig. 7(b), this structure resonates at four frequencies, three of which are in close proximity, just as in Fig. 5(b). In this case, these three resonant frequencies occur at 1.4 GHz, 1.65 GHz, and 2.1 GHz. The extraction shown in Fig. 7(c) reveals that, as previously, the three close resonances resulted in negative permittivity, spanning from 1.4 GHz to 2.45 GHz, which is a bandwidth of 55%. Thus, it is seen that the effect of the two loading pieces of the structure is to pull the electric response to lower frequencies, at the cost of bandwidth. The maximum dimension of the structure is 20 mm, which corresponds to $\lambda/10$ at 1.5 GHz. Thus, minimizing the size of the structure is more critical than increasing the bandwidth. The fourth resonance observed in Fig. 7(b) is at 2.8 GHz. As shown, this resonance is much weaker than in the case of the original structure. As previously, it produced a slight dip in permeability, which is shown to be negative from 2.65 GHz to 2.8 GHz.

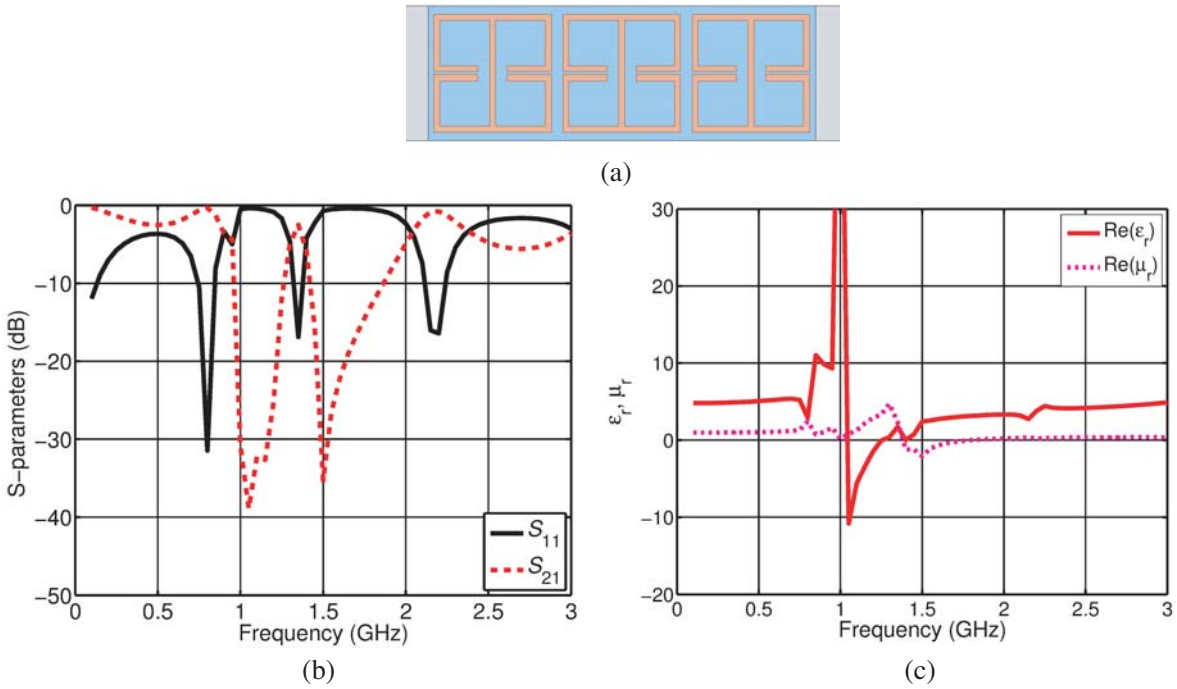

Figure 6. (a) Three unit cells for a structure where a single gap has replaced the two gaps on either side of each unit cell. (b) The reflection and transmission for three unit cells of the structure with a single gap on either side. (c) The extracted permeability and permittivity for three unit cells of the structure with a single gap on either side.

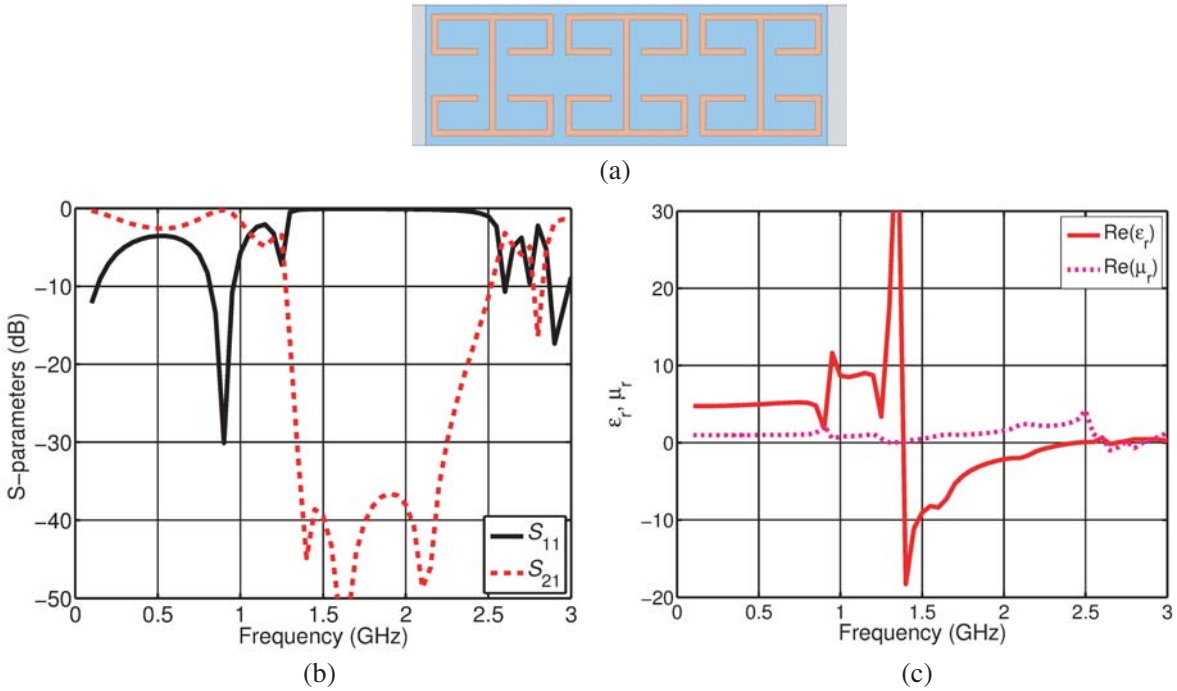

Figure 7. (a) Three unit cells for a structure where the loading element has been removed from either side of the unit cell. (b) The reflection and transmission for three unit cells of the structure with the loading element removed from either side. (c) The extracted permeability and permittivity for three unit cells of the structure with the loading element removed from either side.

4. NOTCH FILTER APPLICATIONS

One of the simplest applications for these unit cells is as a transmission line notch filter. This section will first demonstrate the effectiveness of these unit cells as a notch filter in a finite-width parallel plate waveguide, then in a more practical coaxial transmission line.

4.1. Metamaterial Notch Filter in Parallel Plate Waveguide

To implement the notch filter in a parallel plate waveguide, five sets of three unit cells were milled out on FR-4 epoxy. A length of parallel plate waveguide having a width of 100 mm and a plate separation of 22 mm was also fabricated. A detailed schematic of this fixture is shown in Fig. 8(a). As shown, the length of parallel plate waveguide was fed via a transition section leading from coaxial cable to microstrip to the parallel plate waveguide. Calibration standards were used to mitigate the effect of these transitions on the measured results.

Figure 8(b) shows a photograph of the five sets of three unit cells, arranged at a spacing of approximately 10 mm, to match the y-dimension of the simulated parallel plate waveguide. As shown, a red styrofoam sheet was used at the top and bottom of the unit cells, to maintain the appropriate spacing. The effect of this styrofoam on the measured results is presumed to be negligible, since the foam is primarily air-filled. The calibrated S_{21} resulting from this measurement is shown in Fig. 8(c)

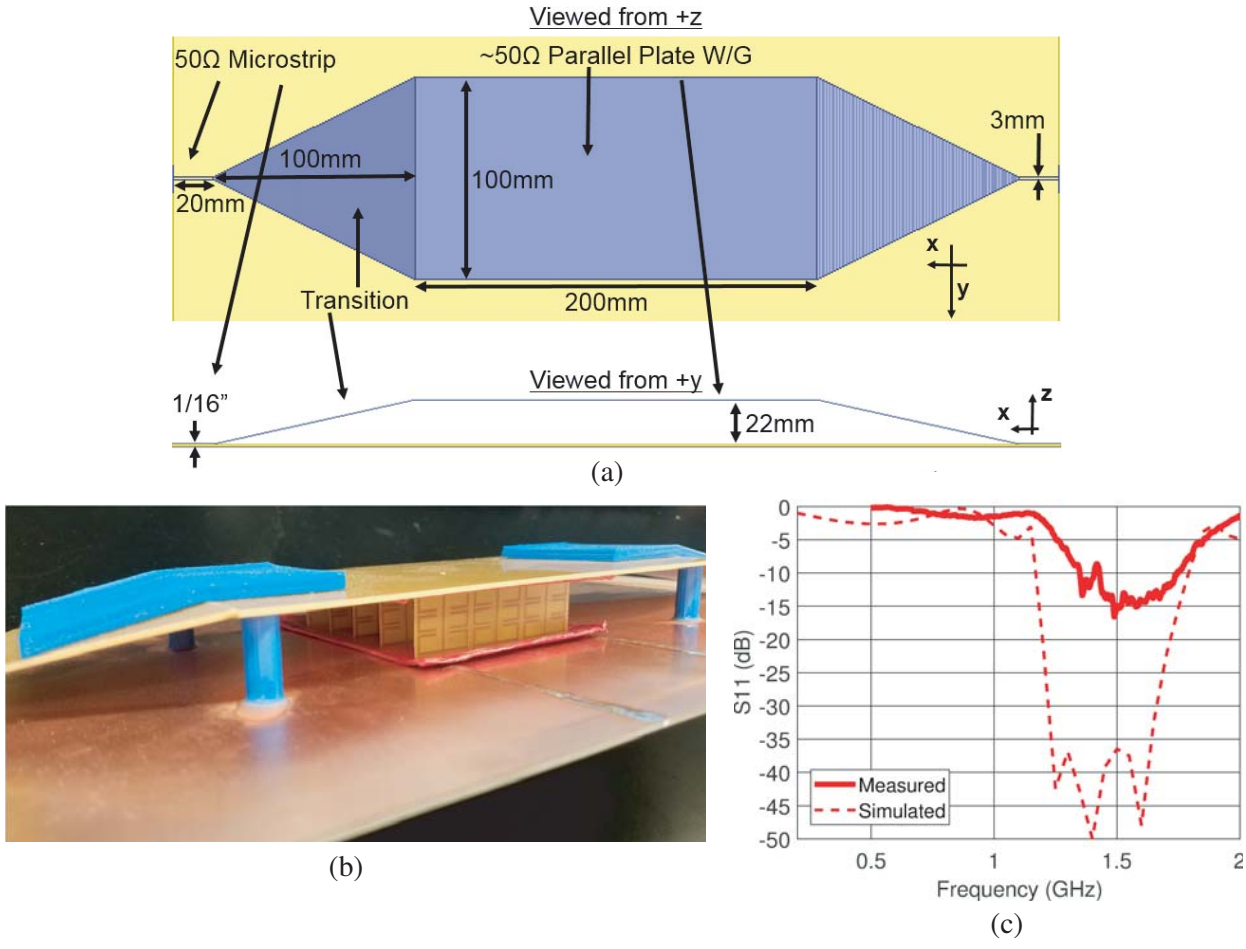

Figure 8. (a) The parallel plate waveguide section used to measure the transmission parameters of the unit cells. (b) A finite-width parallel plate waveguide section with unit cells arranged between the plates. (c) Measured S_{21} for the unit cells in a parallel plate waveguide.

in solid red, along with the simulated S_{21} from the infinite parallel plate case in dashed red. As shown, the measured response is weaker than the simulated. The reason for this discrepancy is that the sides of the waveguide, which were defined as PMC for the sake of efficiency in the simulation, were open in the fabricated case. This led to a significant portion of the field energy fringing around the sides of the guide. These fringing fields failed to interact with the unit cells, thereby diluting their perceived effectiveness.

4.2. Metamaterial Notch Filter in Coaxial Waveguide

Finally, the unit cells were implemented as a notch filter in a coaxial transmission line section, the HFSS model of which is shown in Fig. 9(a). This coaxial waveguide section, which is discussed in great detail in [14], was given an inner radius of 3.175 mm and an outer radius of 26.675 mm. The guide was filled with a dielectric where $\epsilon_r \approx 2$, and the unit cells were inserted radially between the inner and outer conductors.

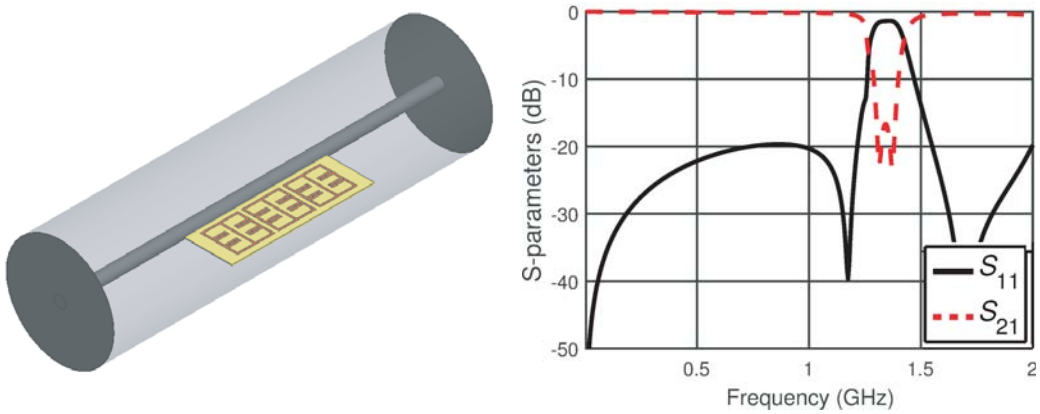

(a) (b)

Figure 9. (a) HFSS model of the three unit cells implemented as a notch filter in a coaxial transmission line. (b) The S-parameters resulting from this simulation.

Figure 9(b) presents the S-parameters resulting from this simulation. As shown, the response of the unit cells in the coaxial transmission line is much narrower than in the case of the infinite parallel plate implementation shown in Fig. 5(b). There are only three visible resonances, one of which occurs very weakly at 1.27 GHz, and two of which are closely spaced at 1.32 GHz and 1.37 GHz.

Though both parallel plate waveguides and coaxial transmission lines support TEM wave propagation, there are several significant ways in which this environment differs from that seen in the original infinite parallel-plate waveguide simulations presented in Fig. 5. Firstly, the images reflected by the PEC and PMC boundaries differ. The parallel plate waveguide has straight PEC and PMC boundaries. These boundaries result in infinitely repeating image currents in both the y-dimension and the z-dimension. In the z-dimension, the PEC boundaries result in alternating reversal of the transverse currents, but consistently-directed normal currents. In the y-dimension, the PMC boundaries result in alternating reversal of the normal currents, but consistently-directed transverse currents. Also, because the PEC and PMC boundaries are planar, the images all have the same size as the actual metamaterial structure.

The coaxial fixture has PEC boundaries, which result in infinitely repeating images in the radial dimension, with alternately reversed transverse currents, and consistently-directed normal currents. However, the curvature of the PEC boundaries in the z- and y-dimensions results in warping of the radial images, as discussed in [14]. For the sake of completeness, it should also be noted that the coaxial fixture has infinitely repeating currents in the azimuthal dimension as well, occurring every 2π radians, and having exactly the same shape and distribution as on the original structure.

The field distribution in the parallel plate case also differs from the coaxial case. Specifically, the

field in an empty parallel plate waveguide is uniformly distributed in both the y-dimension and the z-dimension. However, the field in a coaxial structure decays with the inverse of the radius. Thus, the field is significantly stronger just outside the center conductor than it is just inside the outer conductor. The coaxial test structure also differs in that it was 3D printed of solid ABS plastic, whereas the infinite parallel plate case was vacuum-filled. This may reasonably be expected to shift the response of the structure to lower frequencies.

Finally, and most significantly, a large percentage of the field is allowed to transmit through the empty space around the unit cells without interacting. To demonstrate the significance of this "fill factor effect", an additional simulation was performed, with eight sets of three unit cells arranged around the circumference of the coaxial line section, as shown in Fig. 10(a). The S-parameters resulting from this simulation are shown in Fig. 10(b). As shown, in this case the strong wideband response is restored, with resonances occurring at 1.16 GHz, 1.28 GHz, 1.48 GHz, and 1.89 GHz.

The single-slot coaxial transmission line section was fabricated of ABS plastic using 3D printing, and copper foil was used to achieve conductivity on the appropriate surfaces. Again, calibration standards were also fabricated, to enable post-measurement negation of the transition from the coaxial cable feed to the larger coaxial transmission line section. The fabricated coaxial transmission line structure is shown in Fig. 11(a), with the three unit cells balanced on the edge of the measurement slot.

The reflection resulting from measurement of this coaxial line section loaded with the metamaterial notch filter is shown in Fig. 11(b) in solid black, with the corresponding simulation results shown

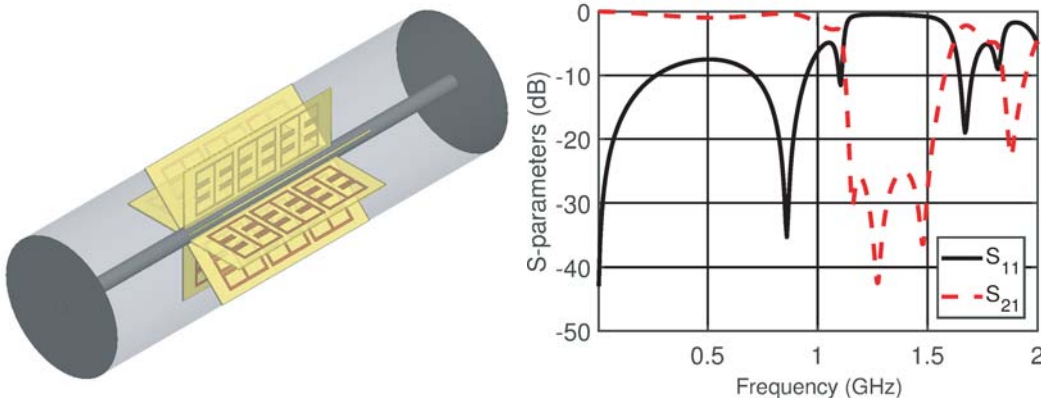

(a) (b)

Figure 10. (a) HFSS model of eight sets of three unit cells implemented as a notch filter in a coaxial transmission line. (b) The S-parameters resulting from this simulation.

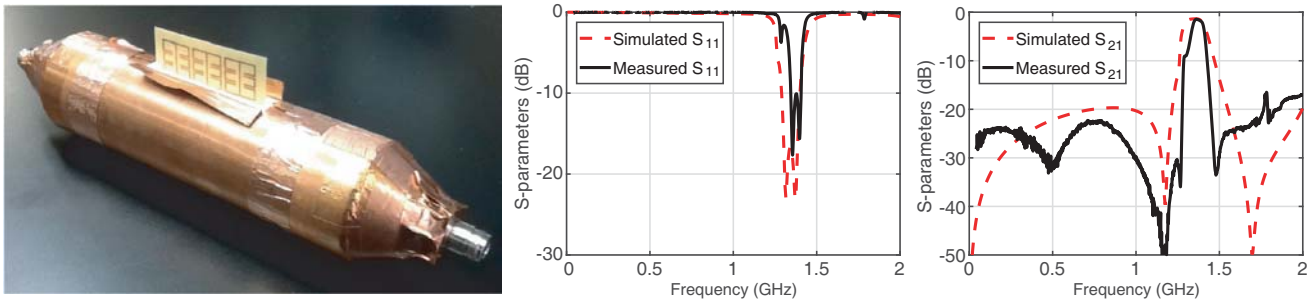

(a) (b) (c)

Figure 11. (a) A 3D printed test fixture, consisting of solid ABS plastic overlaid with copper foil, having a radial slot for a single set of three unit cells. (b) Simulated (dashed red) and measured (solid black) S_{11} for this case. (c) Simulated (dashed red) and measured (solid black) S_{21} for this case.

in dashed red. This plot shows nearly the same features in measurement as in simulation, though the response is slightly narrower. Three resonances are observed in the measured data at 1.29 GHz, 1.36 GHz, and 1.40 GHz, and a fourth, though very weak, appears at 1.79 GHz. Fig. 11(c) shows the corresponding transmission plot.

5. CONCLUSION

A fractal-inspired metamaterial unit cell for notch filter applications has been introduced, and has been shown in simulation to exhibit two distinct frequencies of resonance. Broadband negative permittivity was demonstrated at the first resonance, both through examination of the fields and currents on the structure at that resonance and through mathematical parameter extraction. The second resonance was similarly shown to exhibit negative permeability, though at a frequency where the unit cell is only marginally electrically small. Two simulations presenting small alterations in the unit cell geometry were explored, to observe the effects of various geometrical components. A three-unit-cell structure was shown to exhibit a much wider operative bandwidth than the single unit cell structure. Initial development of this three-unit-cell structure was conducted through HFSS simulation in an infinite parallel plate waveguide. Preliminary measurements were taken in a finite parallel plate waveguide. Finally, the unit cells were both simulated and measured in a coaxial transmission line, and demonstrated better than 10 dB rejection in the band of operation. In applications where a stronger or wider-bandwidth response is required, it was shown through simulation that such could be achieved either through increasing the number of unit cells in the direction of propagation, or by increasing the fill-factor in the guide.

REFERENCES

1. Wongkasem, N., A. Akyurtlu, J. Li, A. Tibolt, Z. Kang, and W. D. Goodhue, "Novel broadband terahertz negative refractive index metamaterials: Analysis and experiment," *Progress In Electromagnetics Research*, Vol. 64, 205–218, 2006.
2. Hudlika, M., J. Machac, and I. Nefedov, "A triple wire medium as an isotropic negative permittivity metamaterial," *Progress In Electromagnetics Research*, Vol. 65, 233–246, 2006.
3. Weldon, T. P., K. Miehle, R. S. Adams, and K. Daneshvar, "A wideband microwave double-negative metamaterial with non-Foster loading," *Proc. IEEE Southeastcon*, 1–5, 2012.
4. Ziolkowski, R. W., "Design, fabrication, and testing of double negative metamaterials," *IEEE Trans. Antennas Propag.*, Vol. 51, No. 7, 1516–1529, 2003.
5. De, T. M., M. Luque, N. R. K. Devarapalli, and C. Christodoulou, "Investigation of bandwidth enhancement in volumetric left-handed metamaterials using fractals," *Progress In Electromagnetics Research*, Vol. 131, 185–194, 2012.
6. Smith, K. L. and R. S. Adams, "A $\lambda_\circ/60$ spherical spiral metamaterial for negative permeability and negative permittivity," *IEEE Int. Symp. on Ant. and Prop. (APSURSI)*, 719–720, 2016.
7. Miyamaru, F., Y. Saito, M. W. Takeda, B. Hou, L. Liu, W. Wen, and P. Sheng, "Terahertz electric response of fractal metamaterial structures," *Phys. Rev. B*, Vol. 77, 045124.1–045124.6, 2008.
8. Li, D. and J. Mao, "Koch-like sided Sierpinski gasket multifractal dipole antenna," *Progress In Electromagnetics Research*, Vol. 126, 399–427, 2012.
9. Smith, K. L., R. S. Adams, and T. P. Weldon, "A novel broadband fractal metamaterial unit cell," *IEEE Int. Symp. on Ant. and Prop.*, 549–550, 2014.
10. Khan, O., Z. Islam, I. Rashid, F. Bhatti, and Q. Islam, "Novel miniaturized Koch pentagonal fractal antenna for multiband wireless applications," *Progress In Electromagnetics Research*, Vol. 141, 693–710, 2013.
11. Li, D. and J. Mao, "Sierpinskized Koch-like sided multifractal dipole antenna," *Progress In Electromagnetics Research*, Vol. 130, 207–224, 2012.
12. Liu, R., A. Degiron, J. J. Mock, and D. R. Smith, "Negative index material composed of electric and magnetic resonators," *Appl. Phys. Lett.*, Vol. 90, No. 26, 263504.1–263504.3, 2007.

13. Szabó, Z., G. Park, R. Hedge, and E. Li, "A unique extraction of metamaterial parameters based on Kramers-Kronig relationship," *IEEE Trans. Microw. Theory Tech.*, Vol. 58, No. 10, 2646–2653, 2010.
14. Shehan, J. W., R. S. Adams, and T. P. Weldon, "Metamaterial measurement in a cylindrical coaxial fixture with consideration for inter-element coupling," *IEEE Radio Sci. Mtg.*, 138–138, 2014.
15. Xu, H., G. Wang, and Q. Peng, "Fractal-shaped complementary electric-LC resonator for bandstop filter," *Progress In Electromagnetics Research*, Vol. 23, 205–217, 2011.
16. Ebrahimi, A., W. Withayachumnankul, S. Al-Sarawi, and D. Abbott, "Dual-mode behavior of the complementary electric-LC resonators loaded on transmission line: Analysis and applications," *J. Appl. Phys.*, Vol. 116, 083705–083705, 2014.